RT E JOURNAL

Experimental investigation and thermographic imaging of geometry-dependent overheating and its effects in PBF-LB/M

Niklas Ostermann[1] · Luca P. M. Bürgel[1] · Marvin Siewert[2] · Christoph Behrens[2] · Tobias Grimm[1] · Vasily Ploshikhin[2] · Jan T. Sehrt[1]

[1] Hybrid Additive Manufacturing (HAM)
Ruhr University Bochum, Universitätsstraße 150, 44801 Bochum
e-mail: Niklas.Ostermann@ruhr-uni-bochum.de, www.ham.ruhr-uni-bochum.de

[2] Airbus Endowed Chair for Integrative Simulation and Engineering of Materials and Processes (ISEMP)
Bremer Center for Computational Materials Science
University of Bremen, Am Fallturm 1, 28359 Bremen
e-mail: behrens@isemp.de, www.isemp.de

https://doi.org/10.58134/fh-aachen-rte_2025_004

Abstract
This experimental study demonstrates a severe challenge in powder bed fusion of metals using a Laser beam (PBF-LB/M). Depending on the geometry of the manufactured part, heat can accumulate and cause significant overheating in critical regions. The inhomogeneous temperature fields influence the thermal history and, thus, the resulting microstructure and porosity. This influences thermal stress and the part properties. Additionally, shrinkage can occur in the same regions for complex parts when multiple part areas merge during the PBF-LB/M process. Specimens with suitable geometry were fabricated from AlSi10Mg and Alloy 718. The thermal behavior was observed using thermographic measurements. The distortion of the specimens was measured and compared to their geometry and the thermographic measurements. A potential approach was investigated where the thermal conditions were stabilized by reducing the Laser power in critical regions. It was observed that the approach resulted in dense material with less distortion, even if the corresponding Laser power led to compromised density in cold areas. Thus highlighting the opportunity of parameter adaption during the build job.

Keywords Additive Manufacturing · PBF-LB/M · Inconel 718 · AlSi10Mg · Thermographic imaging · Heat balance · Geometry

1. Introduction and motivation

Geometry-induced part heating

A key advantage of additive manufacturing (AM) is geometric freedom, especially in Laser-based powder bed fusion (PBF-LB/M). It allows for building complex geometries, which often cannot (or only with high effort) be produced by conventional manufacturing methods. However, inadequate heat transfer to the build plate can cause heat accumulation [1]. Thus, the part geometry, the volumetric energy density, and the layer time affect the potential heat accumulation [2].

The influence of the part geometry can be explained by the powder surrounding the part during the build process. The powder's thermal conductivity differs in magnitudes compared to the conductivity of the solid metal [3,4]. The powder acts as a thermal isolator, and heat is mainly conducted in the part. Therefore, the more powder beneath the current layer relative to the layer's cross-section, the higher the risk of overheating.

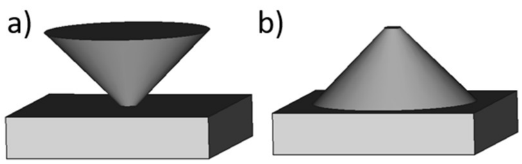

Figure 1: Geometries for the analysis of a different heat-up behavior during PBF-LB/M. a) heat dissipation limited by geometry & b) heat dissipation not limited by geometry

An example of such a geometry was used in the work of Illies et al. [5]: A cone (Figure 1a) with its tip pointing towards the build platform heats up significantly, i.e., the temperature was rising 250 °C above the build platform heating temperature for specimens of 11 mm height with an overhang angle of 42°. If the cone is rotated (Figure 1b; note that this rotated geometry is not discussed [5]), the behavior changes because the heat of new layers is quickly dissipated to the build platform due to the large amount of material underneath.

Consequences of geometry-dependent overheating

If heat accumulates and the material stays hot for a long time, the part is already experiencing an in-situ heat treatment during the build process. The thermal history defines the resulting microstructure of the produced material, i.e., different time-temperature curves may result in different microstructures, e.g., Wenzler et al. observed a non-uniform microstructure due to varying cooling rates aligned with the geometric characteristics [6]. Such effects can be compensated by a feedback loop using EOSSTATE Exposure OT (optical tomography), shown by Nahr et al. using Smart Fusion from EOS GmbH [7]. However, this OT system does not consider the material's emissivity, so no part temperatures are calculated. Additionally, the adaption parameters are not published.

Local overheating at overhangs poses a high risk to process stability if no sufficient support structure is used for overhang angles higher than a critical value. For example, Herzog et al. suggest supporting overhang angles to manufacture Alloy 718 from 50° downwards [8]. But even for less critical overhang angles, the heating affects the melt pool shape and the final surface quality of the part. If heat accumulates at surface regions, unwanted powder adhesion can reduce the surface quality and the part dimensional accuracy [9,10].

Parameter qualification for PBF-LB/M processes is usually based on experimental studies as done in [11]. These aim to identify a set of process parameters (e.g., Laser power, scan speed, hatch distance, and layer thickness) that ensure a stable process resulting in dense material. Geometry-dependent overheating can lead to an increase in the melt pool's depth, as shown by Mohr et al. [12]. The melt pool and, thus, the welding process are very different in the presence of overheating and the qualified process.

Part distortion and overheating

Changes in the melting process can affect the dimensional accuracy of manufactured parts. The part distortion and process parameters are strongly correlated; for instance, it is reported that a decrease in the Laser power results in a decreased distortion [13,14].

In contrast, increasing the global process temperature can lower the induced residual stress (cf., e.g. [15]). Many PBF-LB/M machines have a heated build platform to utilize this effect. In addition, an inhomogeneous temperature field will cause thermal strain.

The aim and scope of this work

This contribution demonstrates the geometry-induced overheating of PBF-LB/M parts through an experimental study utilizing thermographic measurements. The study considers two materials, AlSi10Mg and Alloy 718. Compared to the previously mentioned studies, a different geometry is chosen to highlight that geometry-driven overheating is not only a rare phenomenon. It is investigated whether heat accumulation can be compensated using a process parameter adaption, reducing the energy input in hot regions. Adapting the heat input is an alternative approach to additional cooling times, as used in [1], without extending the manufacturing time. The focus of this study is to identify the impact of heat accumulation and the parameter adaption on the relative density and distortion. The density is analyzed in dedicated regions of the specimens where a different heat accumulation behavior was identified.

2. Material and methods

Powder feedstock

Two different gas-atomized powder materials are used. The aluminum alloy AlSi10Mg represents a very high thermal conductivity example, whereas the nickel-based alloy NiCr19Fe19Nb5Mo3 (Alloy 718) is an example with lower thermal conductivity. AlSi10Mg powder with a nominal particle size distribution from 25 µm to 70 µm was obtained from EOS GmbH (Germany), and Alloy 718 powder with a nominal particle size distribution from 15 µm to 53 µm was obtained from Carpenter Technology Corporation (USA). The morphology of the powder feedstock was analyzed using a scanning electron microscopy (SEM) Zeiss Gemini2 (Carl Zeiss AG, Germany) with an acceleration voltage of 5 kV, a current of 75 pA for AlSi10Mg and 50 pA for Alloy 718, a working distance of 10 mm and a magnification of 500. Predominantly spherical-shaped particles were observed in both powder materials. However, irregularities in shape and satellites also exist (Figure 2).

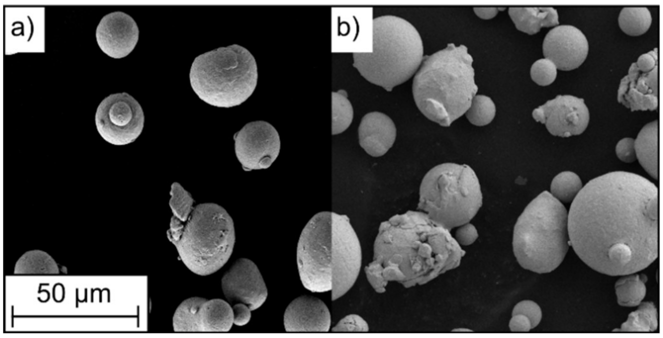

Figure 2: Particle morphology of the powder feedstock a) AlSi10Mg & b) Alloy718 used in this study acquired by SEM.

The particle size distributions were analyzed using Camsizer X2 (Microtrac Retsch GmbH, Germany) with an X Jet module and a dispersion pressure of 250 kPa. The particle size of the Alloy 718 powder has a Gaussian distribution (Figure 3 - blue), while the particle size of the AlSi10Mg powder shows a right-skewed Gaussian distribution (Figure 3 - red). The percentiles D_{10}, D_{50}, and D_{90} for both powders are shown in Table 1: Percentiles of the particle size distribution of powder feedstock used in this study.

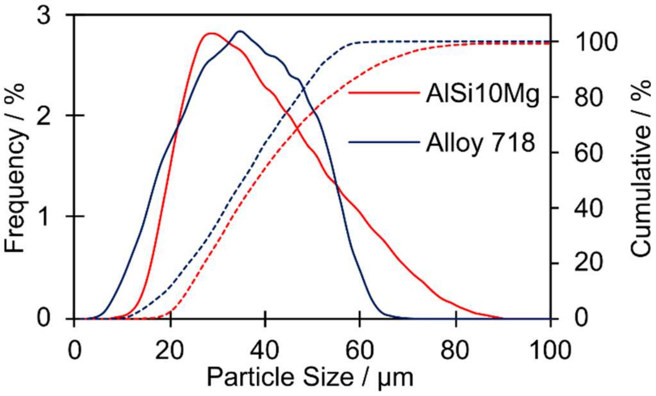

Figure 3: Particle size distribution of the powder feedstock used in this study.

Table 1: Percentiles of the particle size distribution of powder feedstock used in this study.

Powder material	D_{10} / µm	D_{50} / µm	D_{90} / µm
AlSi10Mg	23.5	38.0	61.5
Alloy 718	19.0	35.2	51.0

Additive manufacturing process

The additive manufacturing processes were carried out in an argon atmosphere using an AconityMIDI (Aconity3D GmbH, Germany) PBF-LB/M system with a fiber Laser with a maximum Laser power of 400 W and a wavelength of 1,070 nm. The Laser focus diameter was 80 µm, and a layer thickness (LT) of 60 µm was chosen. Both material parameter sets were prequalified using single tracks and volume specimens. The parameter sets used are summarized in Table 2.

Table 2: Parameter sets used in this study, including Laser power (P), hatch distance (h), scanning speed (v), stripe overlap (so), and the applied volume energy density (VED).

Material	Parameter				
	P	h	v	so	VED
	Unit				
	W	µm	$mm \cdot s^{-1}$	µm	$J \cdot mm^{-3}$
AlSi10Mg	360	119	1,600	150	31.51
Alloy 718	380	97	1,000	100	65.29

The parameters were validated using metallographic preparation, microscopy, and digital imaging of Keyence VHX 6000 (Keyence Corporation, Japan) in three planes on cubic specimens with an edge length of 10 mm. The specimens were manufactured using stripe-based hatching.

Thermographic imaging

The manufacturing process of the following experiments was monitored using the thermographic camera Optris PI 640i (Optris GmbH & Co.KG, Germany) and a Germanium infrared window (Edmund Optics Inc., USA). The camera faces against the recoater direction, and the optical axis of the camera is oriented at an angle of 45° towards the build platform. The thermographic camera has three available temperature ranges (-20 °C - 100 °; 0 °C - 250 °C & 150 °C – 900 °C). The chosen temperature ranges were 0 °C – 250 °C for AlSi10Mg and 150 °C – 900 °C for Alloy 718. However, only one temperature range can be chosen for one experiment.

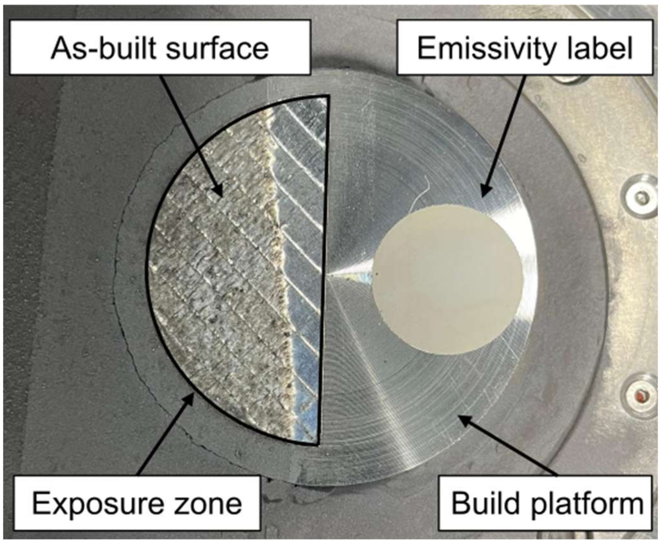

Figure 4: Set-up for emissivity calibration.

The emissivity had to be identified to determine the part temperature. Becker et al. measured the emissivity for additively manufactured surfaces using spectrometers for different wavelength ranges in a separate setup [16].

However, a more simplified approach was chosen for the experiments in this work. The emissivity was measured in the same setup as the measurements during manufacturing to avoid systematic differences between calibration and measurement. With the selected set of parameters, an as-built surface of both materials was manufactured to determine the emissivity of both materials, whereby only half of the build platform was coated with powder, as shown in Figure 4. On the right side (cf. Figure 4), an emissivity label (Optris GmbH & Co.KG, Germany) was placed on the top surface of the build platform. After manufacturing the as-built surface, the build platform was heated to 200 °C for AlSi10Mg and 350 °C for Alloy 718 using the inductive build platform heating of the machine. Maintaining an argon atmosphere throughout the manufacturing and the emissivity calibration process avoids a change of emissivity due to oxidation in the air during the specimen transfer between different setups. The label's emissivity and the Germanium window's transmissivity are known. Thus, the emissivity of the as-built surface can be adapted in the software until the measured temperature of the part and the emissivity label are identical. An emissivity value of 0.13 for AlSi10Mg and 0.36 for Alloy 718 was determined. The measured temperatures during the build jobs were evaluated using the software PIX Connect (Optris GmbH & Co.KG, Germany).

Specimen design

The chosen parameter sets (Table 2) for both materials were used to build 4 cuboid specimens, each with a size of 48 mm × 10 mm × 10 mm. These specimens were manufactured at different heights above the build platform. One specimen was directly placed on the build platform. The specimen is 4 mm higher to guarantee more constant process conditions. The other three specimens were placed 15 mm, 30 mm, and 45 mm above the build platform using an additional pin structure (cf. top right in Figure 5) and two tie bars on the side as a connection to the build platform. Manufacturing the low cross-section pin structures and tie bars without mechanically influencing each other and then connecting them by manufacturing the large cross-section cuboid specimen during the build job provokes overheating and shrinking. The specimens and their positions on the build platform are shown in Figure 5. The exposure order starts with the highest pin structure height and ends with the lowest. This way, the exposure of a cuboid sample is always the last in a layer. Due to the small cross-section of the pin structure, combined with a recoater time of 15 seconds, the influence of varying layer times on the build job height can be neglected. AlMg4.5Mn was selected as the build platform material for the experiment with AlSi10Mg, while C45 carbon steel was selected as the build platform material for Alloy 718. The build platform thickness for all experiments was 18 mm.

Deviation measurement

After manufacturing, the specimens were geometrically measured while connected to the build platform using a GOM Atos Core 200 3D scanning device and evaluated using Zeiss Inspect Optical 3D (Carl Zeiss GOM Metrology GmbH, Germany). To analyze the deformation of the parts, a reference plane was created as the center plane of two fitting planes on the square outer surfaces of specimen 1, which is placed directly on the build platform. Fitting planes for measurement were placed on all outer surfaces of all specimens. However, the normal vector of these was set to be equal to the normal vector of the reference plane. The flatness deviation of these surfaces was measured to identify shrinkage or other distortion.

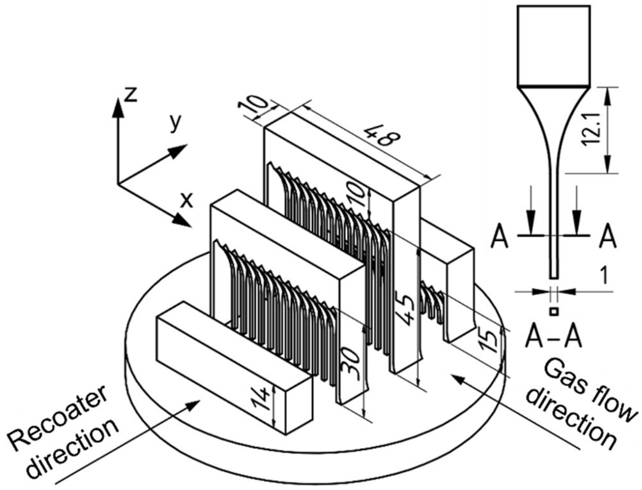

Figure 5: Positions and dimensions of the specimens on the build platform (left); Cross-section of the pin structure (top right).

Both sides of each specimen were analyzed. The surfaces are labeled based on the orientation of their normal vector. If the outside surface faces positive x, the x-axis orientation will be called positive (cf. Figure 5). The sum of the flatness deviations on both specimen sides is called width deviation, considering a potential asymmetry in the flatness deviation measurements.

Relative density analysis

To measure the relative density, a centered 10 mm section of the specimens was cut and metallographically analyzed in three planes using microscopy and digital imaging of Keyence VHX 6000 (Keyence Corporation, Japan).

3. Results and discussion

Parameter validation

A relative density of the validation specimens above 99.8 % was measured. The mean relative density and standard deviation are shown in Table 3.

Table 3: Achieved relative densities for cubic specimens manufactured with the prequalified parameter sets.

Material	Relative density / %	
	Mean	Standard deviation
AlSi10Mg	99.89	0.008
Alloy 718	99.99	0.001

Figure 6 shows the cross-sections of a specimen built with the selected parameter sets for both materials.

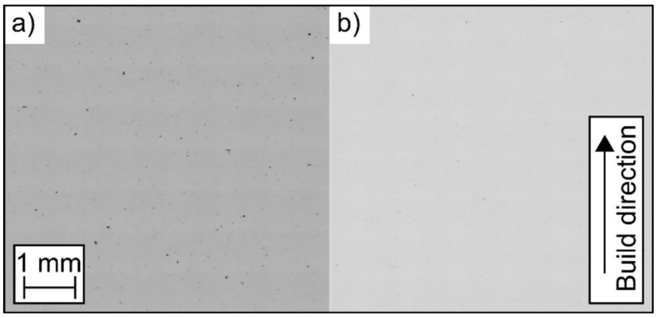

Figure 6: Cross-sections of specimens manufactured with the selected parameter set out of a) AlSi10Mg b) Alloy 718.

Thermographic imaging and overheating analysis

Using thermographic imaging, no significant temperature deviations can be found within the top surface of a single specimen. However, the part temperature influences the part geometry, in this case, pin structure height and material. This is caused by the small cross-section of the pin structures and the resulting low thermal conduction into the build platform. The exposure time for a single layer was measured to be ~7 s for AlSi10Mg and ~12 s for Alloy 718, depending on the stripe orientation.

Figure 7 shows thermographic images of the different specimens manufactured in this study. Higher temperatures are observed for Alloy 718 compared to AlSi10Mg, while higher pin structures lead to higher measured temperatures. The thermographic imaging was analyzed in three batches of ten layers per specimen at each specimen's bottom, center, and top layers. A bottom temperature T_b, a center temperature T_c and an upper layer temperature T_u for each specimen was measured. The images were always captured for the complete layers 1 s after the end of the exposure.

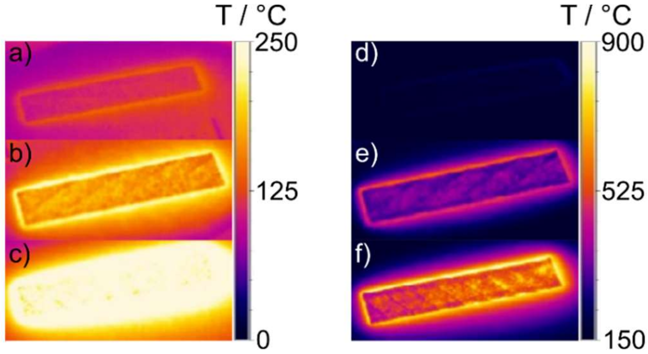

Figure 7: Thermographic imaging of the final layer 1 s after the exposure of specimens manufactured out of AlSi10Mg with a pin structure height of a) 0 mm, b) 15 mm, and c) 45 mm; and out of Alloy 718 with a pin structure height of d) 0 mm; e) 15 mm and f) 45 mm.

Comparing the measured temperatures at a single specimen's bottom, center, and upper regions, a different behavior for the specimen manufactured directly on the build platform was observed compared to the other three specimens.

The temperature of the specimen manufactured directly on the build platform increases with the build height, i.e.

$$T_b < T_c < T_u$$

This is possible due to the overall heating of the build platform and the machine. However, the temperatures for specimens on pin structures are observed to be the highest at the bottom area of the specimen and decrease slightly with increasing build height (cf. Figure 8), i.e.

$$T_u < T_c < T_b$$

This is possible due to the increasing volume of the cuboid sample. The energy input remains constant while the heat dissipation into the powder bed and through the cross-section of the specimen and the tier bars into the build platform increases, altering the equilibrium state of the heat in the sample towards lower temperatures.

All specimens show higher temperatures with increasing pin structure height. For AlSi10Mg, the part temperature increased from ~100 °C for 0 mm pin structure height to up to 260 °C for 45 mm pin structure height (comparing T_b against T_b, T_c against T_c and T_u against T_u). The measured part temperature for AlSi10Mg starts to show a saturation behavior for pin structure heights > 30 mm. This is possibly due to the high heat conductivity of AlSi10Mg. In contrast, the temperature of specimens manufactured out of Alloy 718 increased from 145 °C to ~575 °C. Here, the higher temperature values can be explained by higher applied VED and the lower heat conductivity of Alloy 718 [17] compared to AlSi10Mg [18].

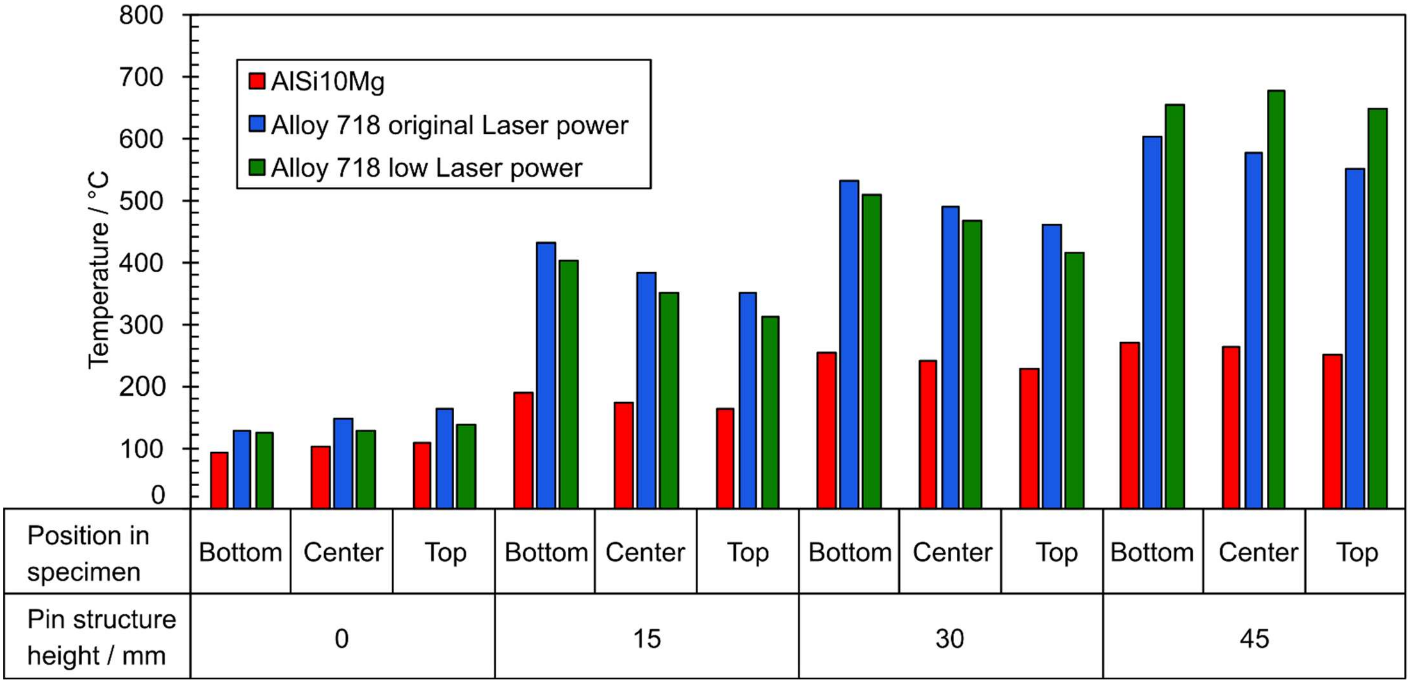

Figure 8: Measured part temperature for specimens manufactured in this study.

Adaption of Laser power

For Alloy 718, significantly higher temperatures are identified for specimens on high pin structures after the exposure, leading to higher temperatures before the exposure of the next layer. Therefore, the temperature difference between the underlying part and the melting temperature gets significantly smaller. Thus, less energy is required to melt the already hot material. This leads to the assumption that a lower VED can be applied while producing dense specimens. The experiment was repeated for Alloy 718 with a lower VED to investigate this assumption. The hatch distance was not increased to ensure comparability by maintaining the hatching paths. Increasing the scanning speed would lead to shorter layer times and different thermal conditions. Thus, only the Laser power was adjusted.

The Laser power was reduced from 380 W to 240 W, a 36.8 % reduction. Therefore, the VED decreased by the same proportion and is now 41.24 J mm^{-3}. The Laser power of 240 W was chosen based on the single-track experiment during parameter qualification. 240 W was the lowest Laser power, which reliably led to continuous single tracks using a scanning speed of 1000 mm/s. However, the Laser power was only reduced for the cuboid specimens to ensure dense material in the pin structure regions. The pin structures were still manufactured using the original parameter set.

For Alloy 718, only a slight reduction in part temperature was observed for most specimens, comparing the temperatures of parts manufactured with and without reduced Laser power (cf. Figure 8). This is possibly due to the Laser power being reduced only in the specimen area. The energy input during the manufacturing of the pin structures was the same, setting the base temperature of the part. However, the measured temperature for the pin structure height of 45 mm is higher for the lower Laser power of 240 W compared to the original Laser power of 380 W. This cannot be explained by the energy input but by the changed surface condition in the case of the hot specimens. This can result in a different emissivity value. Thus, the measurement of the 45 mm specimen is expected to be less accurate. Therefore, an analysis of the powder temperature was carried out.

By analyzing the temperature of the powder layer before the exposure, a higher temperature was measured for the specimen built with higher Laser power than the specimen built with lower Laser power. It must be made clear that temperatures are not measured directly. Instead, the radiation is measured, and using the calibrated emissivity value, the radiation is transferred into temperatures. The emissivity parameter is, after calibration, a fixed value. However, the emissivity depends on many factors, such as temperature and surface topology. Therefore, the observed effect, which is that the temperature is higher in the specimen scanned with reduced Laser power, might be due to the difference in the effective emissivity value. Thus, it is assumed that the specimen with a pin structure height of 45 mm behaves similarly to specimens with a pin structure height of 15 mm or 30 mm regarding the influence of used Laser power on part temperature. A surface topology and reflectivity change of the top surfaces of the specimens can be observed by visual specimen inspection (Figure 9). This leads to the assumption that the emissivity of additively manufactured surfaces is highly dependent on the process condition and cannot be determined using a single sample. However, the trends in part temperatures

- except for the samples manufactured out of Alloy 718, with a pin structure height of 45 mm - can be explained by the specimen geometry, the material properties, and the used parameter sets.

Figure 9: Top surface of specimens manufactured out of Alloy 718 using the original Laser power of 380 W

Distortion measurement and analysis

Distortion is observed in the transition zone from the pin structure to the bulk. Figure 10 shows the scanned specimens for all three experiments and visualizes the measured flatness deviation on one side of the specimens. A more considerable distortion is observed for specimens on high pin structures than those with a low pin structure height.

A larger negative deviation is localized in the transition zone between the pin structure and the specimen. This indicates that the first layers of the cuboid specimen exert enough tension on the pin structure to deform it significantly during the process. Multiple pin structures are sometimes deformed even to touch each other (Figure 11).

A dependence of the distortion, measured as flatness deviation, on the pin structure height, is observed (Figure 12a). The flatness deviation shows asymmetric behavior. However, the number of manufactured specimens does not allow for identifying regularities regarding asymmetric displacement behavior.

A dependence of the width deviation on pin structure height is also observed for all three experiments (Figure 12b). However, for AlSi10Mg, the measured width deviation does not change significantly between the specimens with a pin structure height of 30 mm and 45 mm. For these specimens, the increase in the inter-layer temperature was also low (cf. Figure 8).

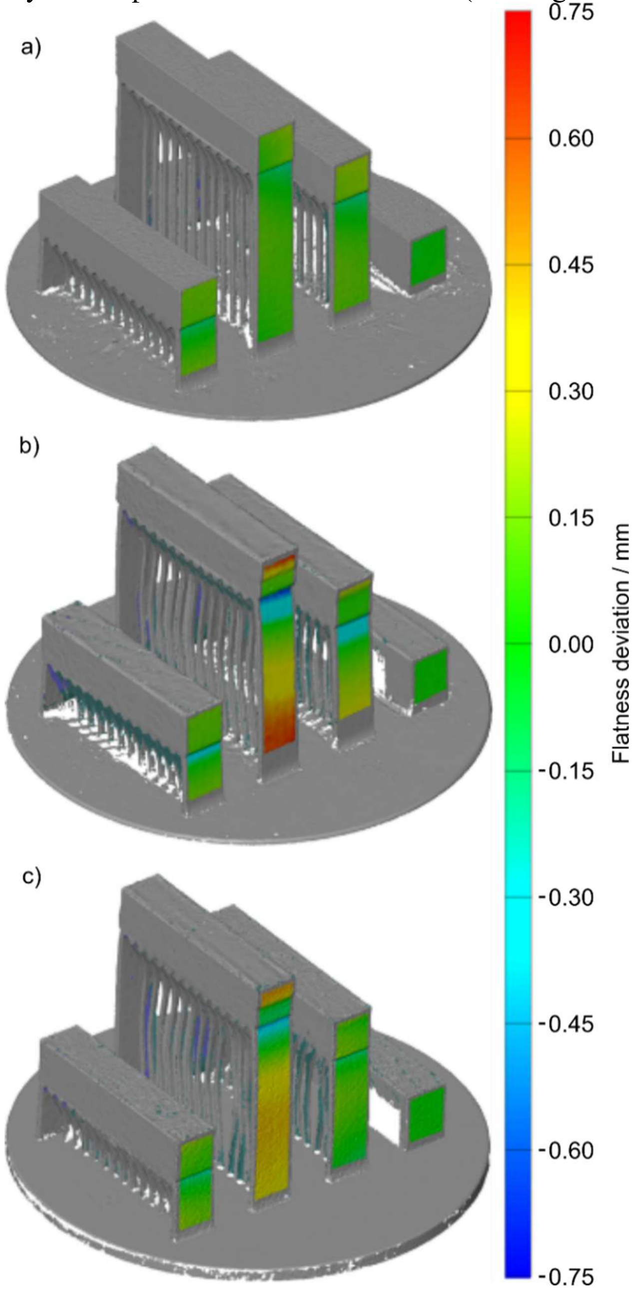

Figure 10: Visualized flatness deviation for specimens with different pin structure heights, manufactured out of a) AlSi10Mg using the original Laser power of 360 W; b) Alloy 718 using the original Laser power of 380 W & c) Alloy 718 using the lower Laser power of 240 W.

A possible explanation is that reduced material properties due to overheating make the specimen more susceptible to distortion. Thus, the width deviation would only increase with rising temperatures.

Uzan et al. reported that the yield and ultimate tensile stress dropped significantly for additively manufactured AlSi10Mg when increasing the test temperature above 200 °C [19].

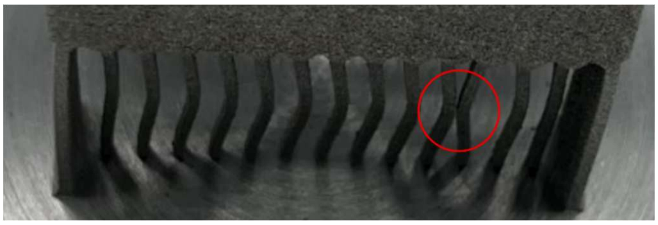

Figure 11: Deformed pin structures of the specimen with a pin structure height of 15 mm manufactured out of Alloy 718 using the original Laser power of 380 W.

The width deviation for specimens manufactured out of Alloy 718 with the original parameter set shows a significant increase in width deviation over increasing pin structure height. An increase in pin structure height from 15 mm to 30 mm increases the width deviation by 35 %, while an increase in pin structure height from 30 mm to 45 mm results in an increase in width deviation of 65 %.

Again, the substrate's material properties could be weakened in the presence of heat accumulation (as Uzan et al. reported for AlSi10Mg [19]). Consequently, the substrate would be more prone to deform.

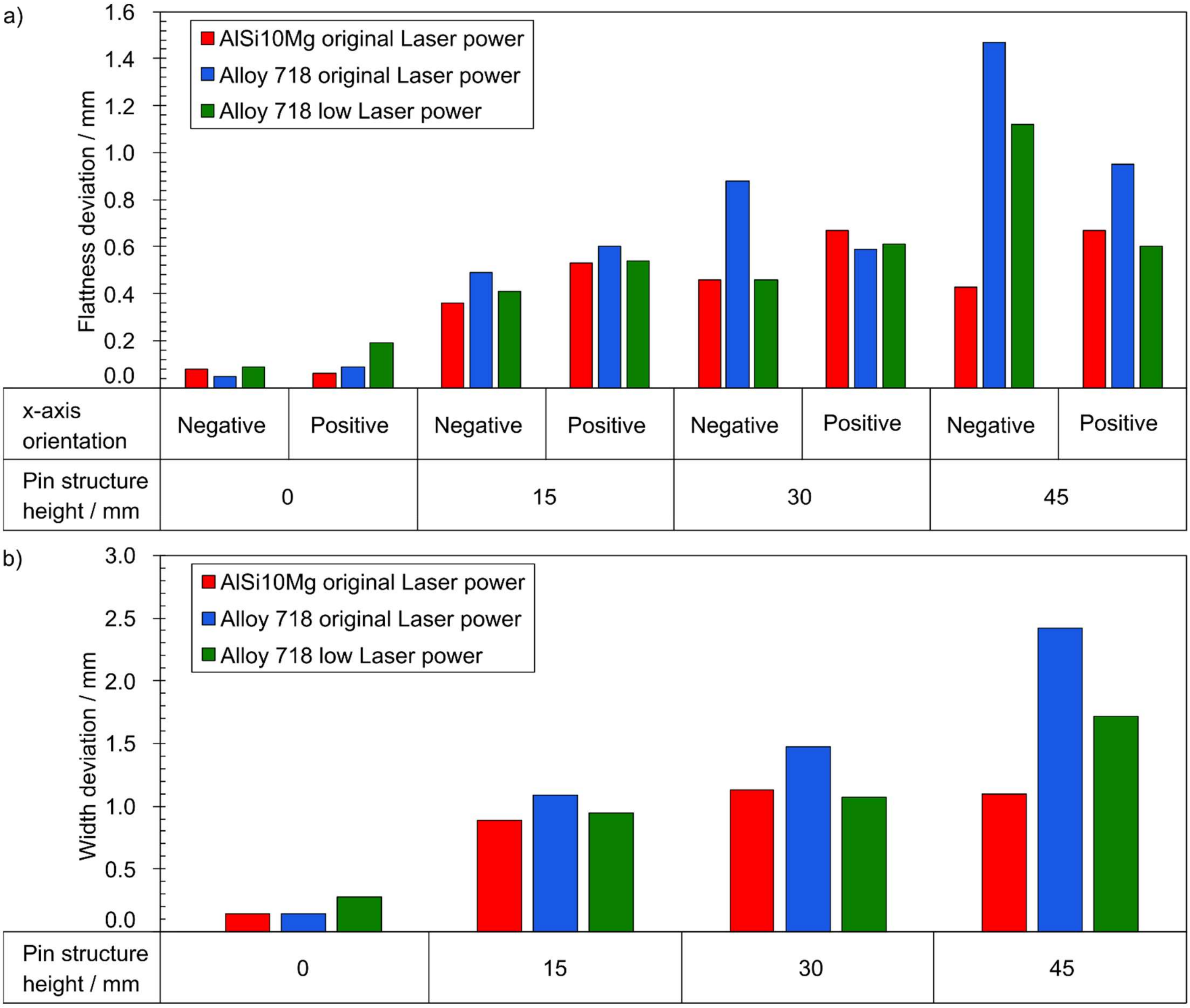

Figure 12: a) measured flatness deviation using Zeiss Inspect Optical 3D, b) calculated width deviation of the specimens for both materials.

An explanation for the distortion behavior of the tie bars could be that the specimen temperatures above 200 °C could imply that the first layers of the cuboid specimen are less rigid. Hence, they cannot withstand the forces of the tie bars against the direction of shrinkage. Thus, the reduced bending stiffness of the tie bars at greater pin structure heights may have no influence.

Another possible mechanism is that the tie bars' bending stiffness around the y-axis is reduced with increasing pin structure height.

Reducing the Laser power while manufacturing specimens out of Alloy 718 greatly influences the width deviation. While the width deviation still increases with increasing pin structure height, a reduction of width deviation of up to 29 % compared to the original parameter set is observed. According to the literature, reducing power can decrease distortion ([13,14]).

The temperature of the Alloy 718 specimens manufactured with and without reduced Laser power is not significantly different. Thus, the reduction in the width deviation by the Laser power reduction is not explained by part temperature. Therefore, reducing the Laser power might reduce the residual stress from the melting process itself.

Another explanation for the dependency of flatness deviation on pin structure height could be that the melt pool size may increase with higher part temperatures (as reported by Mohr et al. [12]), leading to additional stress being applied deeper into the material.

However, to truly understand the mechanism explaining the distortion behavior, detailed process simulations, and more experimental work are necessary, which are beyond the scope of this work.

Relative density analysis

Analyzing the achieved relative densities of the manufactured specimens, mostly high values of around 99.9 % were measured (Table 4). Only the specimen manufactured out of Alloy 718 directly on the build platform using the lower Laser power of 240 W has a significantly lower relative density of 99.27 %, indicating that this parameter is unsuitable for the manufacturing of Alloy 718 when no heating of the part is applied.

Table 4: Achieved relative densities of specimens manufactured in this study.

Material	Laser power	Pin structure height / mm			
		0	15	30	45
		Mean relative density / %			
AlSi10Mg	Original 360 W	99.90	99.94	99.86	99.89
Alloy 718	Original 380 W	99.94	99.99	99.98	99.97
Alloy 718	Low 240 W	99.27	99.97	99.98	99.98

During metallographic analysis, mainly small spherical-shaped pores are observed as defects. However, the specimen manufactured directly on the build platform out of Alloy 718 using the lower Laser power shows mostly defects with an irregular shape and significantly bigger size compared to other specimens out of Alloy 718 (Figure 13).

This highlights the challenges in using adaptive process parameters in complex shapes: the reduced Laser power can lead to a lack of fusion porosity if the heat accumulation is less than expected.

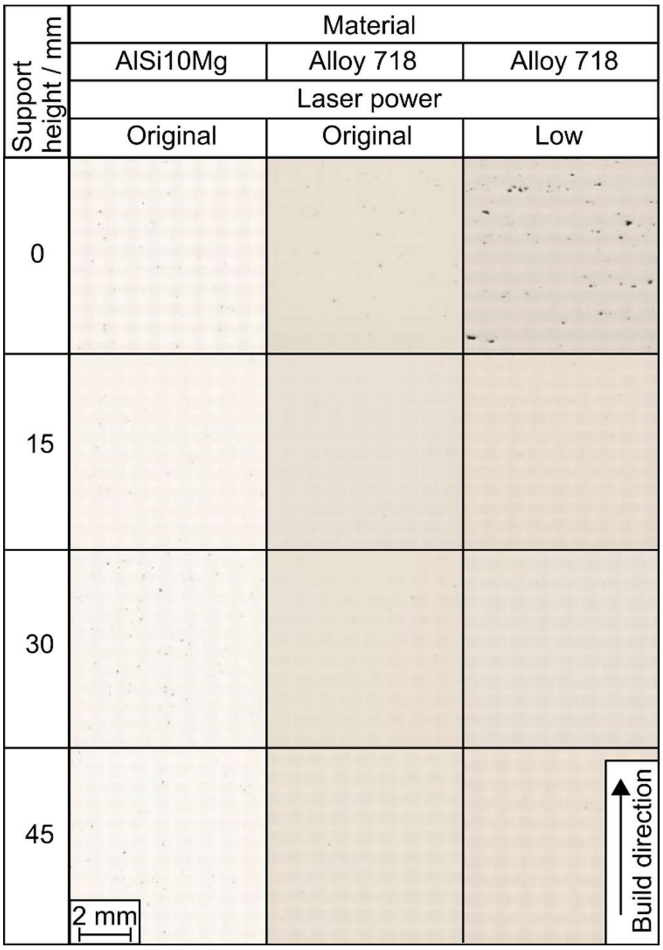

Figure 13: Cross-sections of specimens manufactured in this study.

4. Conclusion and outlook

This study shows that part geometries highly influence the thermal conditions during the PBF-LB/M process. Still, for Alloy 718, it was shown that a reduced Laser power reduced the distortion of the manufactured specimens by up to 29 %, demonstrating the potential of parameter adaption in PBF-LB/M. However, the same parameters led to an increased porosity in the absence of significant heat accumulation. Overheating and shrinkage due to low bending stiffness may appear in the same regions in complex parts. This work shows the potential to adapt the Laser power based on the overheating to reduce shrinkage.

The results of this work show that overheating in PBF-LB/M is not only an effect that needs to be controlled. In this work, no significant reduction in part temperature was achieved, while distortion was drastically reduced. This may only work due to high part temperatures. Therefore, overheating offers the opportunity to adapt parameters to improve part quality.

Thus, the potential benefits of parameter adaption based on part temperature are expanded. Future work should investigate the capabilities and possibilities of parameter adaption even more. However, it seems useful to qualify different parameters for different part temperatures using build platform heating since low VED parameter sets may only work for high part temperatures.

Additionally, it must be clear which parameter set should be used. Thus, the part temperature during the process must be calculated using a thermal simulation or measured using pyrometric or thermographic measurements. These measurements imply the challenge of emissivity measurements since the emissivity depends on the surface condition of the part relative to the measuring device and is also dependent on the part temperature. Quotient pyrometry could be suitable for these measurements, as the temperature is calculated by the ratio of the measured emission at two wavelengths. It is assumed that the emissivities for both wavelengths change by the same ratio when, for example, the surface topology of the measured object changes. However, the applied powder layer before exposure can also be used for this kind of measurement, requiring only calibration for the used powder at different temperatures, as the topology and oxidation state of the powder layer should be more consistent over a single build job [16]. Nevertheless, the influence of process conditions on the emissivity of additive-manufactured surfaces should be further investigated.

5. Acknowledgments

The research project IGF 22690 N "Reduktion des in-situ Verzugs und der Konturüberhöhung durch material- und geometriespezifische Parameteranpassung im PBF-LB/M-Prozess" is supported by the Federal Ministry of Economic Affairs and Climate Action the German Federation of Industrial Research Associations (AiF) as part of the program for promoting industrial cooperative research (IGF) based on a decision by the German Bundestag. The project is carried out at the research institutes ISEMP and HAM.

6. Contributions

N.O.: Specimen design, Experimental design, methodology, data curation, formal analysis, writing-original draft

L.B.: Experimental design, methodology, data curation, formal analysis, writing-original draft

M.S.: Specimen design, writing-original draft

C.B.: Experimental design, writing-original draft

T.G.: writing-review and editing

V.P.: project administration, funding acquisition

J.T.S.: resources, writing-review and editing, supervision, project administration, funding acquisition

All authors: Project Management, technical consultant

References

[1] Ranjan R, Ayas C, Langelaar M, et al. Controlling local overheating in topology optimization for additive manufacturing. Struct Multidiscip Optim 2022; 65: 162. doi:10.1007/s00158-022-03258-1

[2] Kusano M, Watanabe M. Controlling heat accumulation through changing time per layer in Laser powder bed fusion of nickel-based superalloy. J Manuf Process 2024; 131: 187–198. doi:10.1016/j.jmapro.2024.09.001

[3] Wei LC, Ehrlich LE, Powell-Palm MJ, et al. Thermal conductivity of metal powders for powder bed additive manufacturing. Addit Manuf 2018; 21: 201–208. doi:10.1016/j.addma.2018.02.002

[4] Zhang S, Lane B, Whiting J, et al. On thermal properties of metallic powder in Laser powder bed fusion additive manufacturing. J Manuf Process 2019; 47: 382–392. doi:10.1016/j.jmapro.2019.09.012

[5] Illies O, Li G, Jürgens J-P, et al. Numerical modelling and experimental validation of thermal history of titanium alloys in Laser beam melting. Procedia CIRP 2018; 74: 92–96. doi:10.1016/j.procir.2018.08.046

[6] Wenzler DL, Bergmeier K, Baehr S, et al. A Novel Methodology for the Thermographic Cooling Rate Measurement during Powder Bed Fusion of Metals Using a Laser Beam. Integrating Mater Manuf Innov 2023; 12: 41–51. doi:10.1007/s40192-023-00291-w

[7] Nahr F, Novotny T, Kunz D, et al. Advanced process control in Laser-based powder bed fusion–Smart Fusion feedback-loop control as a path to uniform properties for complex structures? J Mater Res Technol 2025; 34: 604–618. doi:10.1016/j.jmrt.2024.12.014

[8] Herzog D, Asami K, Scholl C, et al. Design guidelines for Laser powder bed fusion in Inconel 718. J Laser Appl 2021; 34: 012015. doi:10.2351/7.0000508

[9] Kempen K, Welkenhuyzen F, Qian J, et al. Dimensional accuracy of internal channels in SLM produced parts. 2014

[10] Calignano F, Manfredi D. Production of overhanging structures by DMLS. London: Taylor & Francis Group; 2013

[11] Ahmed N, Barsoum I, Haidemenopoulos G, et al. Process parameter selection and optimization of Laser powder bed fusion for 316L stainless steel: A review. J Manuf Process 2022; 75: 415–434. doi:10.1016/j.jmapro.2021.12.064

[12] Mohr G, Scheuschner N, Hilgenberg K. In situ heat accumulation by geometrical features obstructing heat flux and by reduced inter layer times in Laser powder bed fusion of AISI 316L stainless steel. Procedia CIRP 2020; 94: 155–160. doi:10.1016/j.procir.2020.09.030

[13] Abhishek S, Anand Kumar S, Rao S. Multi-scale modelling for optimization of process parameters of Laser powder bed fusion processed Inconel 718 surrogate part. Eng Fail Anal 2024; 155: 107713. doi:10.1016/j.engfailanal.2023.107713

[14] Xie D, Lv F, Yang Y, et al. A Review on Distortion and Residual Stress in Additive Manufacturing. Chin J Mech Eng Addit Manuf Front 2022; 1: 100039. doi:10.1016/j.cjmeam.2022.100039

[15] Mertens R, Dadbakhsh S, Humbeeck JV, et al. Application of base plate preheating during selective Laser melting. Procedia CIRP 2018; 74: 5–11. doi:10.1016/j.procir.2018.08.002

[16] Becker T, Stark T, Arduini M, et al. Knowing the spectral directional emissivity of 316L and AlSi10Mg PBF-LB/M surfaces: gamechanger for quantitative in situ monitoring. Prog Addit Manuf 2024; 9: 695–704. doi:10.1007/s40964-024-00665-2

[17] Marques A, Cunha Â, Silva MR, et al. Inconel 718 produced by Laser powder bed fusion: an overview of the influence of processing parameters on microstructural and mechanical properties. Int J Adv Manuf Technol 2022; 121: 5651–5675. doi:10.1007/s00170-022-09693-0

[18] Sélo RRJ, Catchpole-Smith S, Maskery I, et al. On the thermal conductivity of AlSi10Mg and lattice structures made by Laser powder bed fusion. Addit Manuf 2020; 34: 101214. doi:10.1016/j.addma.2020.101214

[19] Uzan NE, Shneck R, Yeheskel O, et al. High-temperature mechanical properties of AlSi10Mg specimens fabricated by additive manufacturing using selective Laser melting technologies (AM-SLM). Addit Manuf 2018; 24: 257–263. doi:10.1016/j.addma.2018.09.033